Original Article

Low-to-high b value DWI ratio approaches in multiparametric MRI of the prostate: feasibility, optimal combination of b values, and comparison with ADC maps for the visual presentation of prostate cancer

Yin Xi[1], Alexander Liu[2], Franklin Olumba[2], Parker Lawson[2], Daniel N. Costa[1,3], Qing Yuan[1], Gaurav Khatri[1], Takeshi Yokoo[1,3], Ivan Pedrosa[1,3,4], Robert E. Lenkinski[1,3]

[1]Department of Radiology, [2]Medical School, [3]Advanced Imaging Research Center, [4]Department of Urology, UT Southwestern Medical Center, Dallas, TX, USA

Correspondence to: Yin Xi, PhD. Department of Radiology, UT Southwestern Medical Center, 5323 Harry Hines, Dallas, TX 75390-9061, USA. Email: yin.xi@UTSouthwestern.edu.

Background: Diffusion-weighted imaging (DWI) is considered by experts as one of the key elements in multi-parametric magnetic resonance imaging (mpMRI) employed in oncological studies outside the brain. A low-to-high b value ratio DWI has been proposed as an approach to decrease acquisition time and simplify the analysis of DWI data without the need to use a mathematical model.

Methods: Forty-three men with biopsy-proven prostate cancer (PCa) who underwent mpMRI of the prostate were included. Apparent diffusion coefficient (ADC) maps were created in the MRI scanner using a mono-exponential algorithm [b value (× number of averages) =0 (×1), 10 (×1), 25 (×1), 50 (×1), 100 (×1), 250 (×1), 450 (×1), 1,000 (×2), 1,500 (×3), and 2,000 (×5) s/mm^2]. DWI ratio images were calculated with three previously estimated optimal b value combinations: (I) b=100 and b=1,000 s/mm^2 (R1); (II) b=100 and b=1,500 s/mm^2 (R2); and (III) b=100 and b=2,000 s/mm^2 (R3). For quantitative analysis, contrast-to-noise ratio (CNR) between normal and cancerous tissue was compared between the ADC maps and the DWI ratio images in terms of noninferiority. For qualitative analysis, two radiologists read all images in a randomized order without knowing whether the presented image was an ADC map or a DWI ratio image. All images were scored in terms of artifacts, cancer conspicuity and overall image quality with a 5-point scale. Agreement between the readers was assessed by weighted kappa statistics. Agreement was considered as poor when kappa <0.4, fair to good when kappa >0.4 and <0.75 and excellent when kappa >0.75. Mean scores were compared between ADC and each of the DWI ratio images. Agreement between ADC maps and DWI ratio based synthetic ADC were assessed by intraclass correlation (ICC). Values less than 0.5, between 0.5 and 0.75, between 0.75 and 0.9, and greater than 0.90 were indicative of poor, moderate, good, and excellent reliability, respectively. Median difference between low and intermediate/high risk were tested.

Results: Quantitative analysis shows DWI ratio images were not inferior to ADC maps quantitatively [P=0.0298 (ADC *vs.* R1), <0.0001 (ADC *vs.* R2) and <0.0001 (ADC *vs.* R3)]. Qualitatively, DWI ratio images were no more than 0.5 point on Likert scale lower than ADC in overall quality [P=0.0043 (ADC *vs.* R1), <0.0001 (ADC *vs.* R2), <0.0001 (ADC *vs.* R3)]. Reader agreement for the qualitative analysis was good to excellent (weighted kappa =0.4–0.7). Agreement between ADC maps and the synthetic ADC's were excellent. Significant difference between low and intermediate/high risk were found in all measurements on average (all P values <0.05).

Conclusions: We presented an analytical method for searching for the optimal combination of high and low b values for DWI ratio images in terms of minimizing CNR between cancer and surrounding benign tissues. Optimized DWI ratio images are comparable both quantitatively and qualitatively to ADC maps for the interpretation of DWI data in the context of prostate mpMRI.

Keywords: Diffusion-weighted imaging ratio image (DWI ratio image); optimal b values; apparent diffusion coefficient (ADC); multi-parametric magnetic resonance imaging (mpMRI); prostate cancer (PCa)

Submitted May 07, 2018. Accepted for publication May 16, 2018.
doi: 10.21037/qims.2018.06.08
View this article at: http://dx.doi.org/10.21037/qims.2018.06.08

Introduction

Diffusion-weighted imaging (DWI) is considered by experts as one of the key elements in multi-parametric magnetic resonance imaging (mpMRI) employed in oncological studies outside the brain (1,2). Cancer detection with DWI is based on the characteristic of increased cellularity of malignant tissues relative to benign tissues, which results in reduced diffusion of water and lower apparent diffusion coefficient (ADC) values. In particular, DWI has been shown to improve cancer detection in the prostate (3-7), with lower ADC values observed in cancerous tissues compared to surrounding benign prostate tissue (8-10). Furthermore, cancer ADC values correlate inversely with the Gleason grade (7).

Arguably, the simplest and most widely used approach to obtain and analyze DWI data is the acquisition of a limited number of images with different b values (the magnitude × duration product of the diffusion-sensitizing gradient), and the subsequent fitting of the signal intensity decay observed at increasing b values to a mono-exponential decay to yield an ADC. A shortcoming of this approach is the assumption that the water diffusion in tissue is a random process (Gaussian in nature). Alternatively, more complicated models include the contribution of the intravoxel incoherent motion (IVIM) arising from pseudo-diffusion of water through randomly oriented capillaries to the MRI signal at very low b values (3,11,12). Similarly, other models such as Diffusion kurtosis consider a non-Gaussian diffusion and may be more appropriate (13-16).

Images acquired with high b values improve the detection of prostate cancer (PCa) by increasing cancer conspicuity and reducing the influence of capillary perfusion (17-27). However, such high b value images may also suffer from susceptibility artifacts as well as a decreased signal-to-noise ratio (SNR) (28-31). Iima and Le Bihan reported on the use of two key b values and synthetic ADC images for visualizing and characterizing cancers (16). That is, key b values can be found to maximize sensitivity to the change in diffusion parameters. The synthetic ADC image, which is a normalized ratio of signal intensities observed in two key b value images (i.e., one acquired at low b value and another acquired at high b value) has been proposed as an approach to decrease acquisition time and simplify the analysis of DWI data without the need to use a mathematical model (16). These authors went one step further in proposing the use of a parameter called the signature index (Sindex), which is a 'relative' distance type measurement that measures the relative distance from the observed signals to each of the signature signals (for example, signature signals calculated a priori for benign and malignant tissues). Such a Sindex can be a soft classification of tissue characteristic. Theoretical treatments of it as well as examples of its application in a 9-L glioma in a rat brain indicated the potential utility, short acquisition time, as well as the simplicity of this methodology (16).

The goal of this study was to optimize a low-to-high b value diffusion-weighted image (DWI) ratio approach in optimizing visual presentation of PCa and compare it against conventional ADC maps both qualitatively and quantitatively.

Methods

To carry out this evaluation, we first developed an analytical equation for the contrast-to-noise ratio (CNR) on DWI ratio images and determined the optimal b values based on reference diffusion values from normal and cancerous tissues. Next, we completed two sets of analysis using clinical mpMRI examinations in patients with PCa: (I) quantitative analysis: a comparison of the CNR between DWI ratio images and ADC maps; and (II) qualitative analysis: assessment of subjective image quality and lesion conspicuity on DWI ratio images and ADC maps; lastly, we compare the DWI ratio based synthetic ADC to the ADC maps in terms of agreement and difference across lesion subtypes.

CNR is defined as the difference in mean values between cancer and the uninvolved peripheral zone (see definition below) divided by the standard deviation of the signal in the peripheral zone. A higher CNR suggests better cancer-

Table 1 Reference values for pure tissue diffusion (D), pseudo-diffusion (Dp) and perfusion fraction (f) (BLINDED reference)

Variable	D (×10^{-3} mm^2/s)	f (%)	Dp (×10^{-3} mm^2/s)
Cancer	0.68	17	45
PZ	1.76	13	45

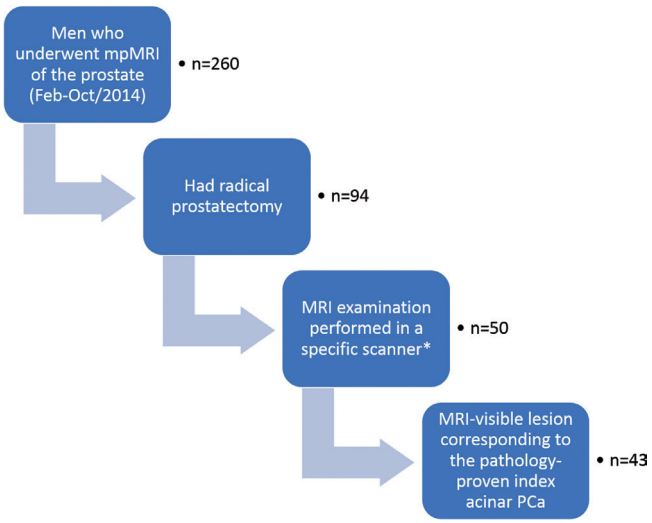

Figure 1 Flowchart for patient inclusion. *, 3 Tesla dual-transmit MRI Scanner (Achieva, Philips). mpMRI, multiparametric MR imaging; PCa, prostate cancer.

peripheral zone differentiation. The following analysis was carried out to determine the optimal high-low b value combination that yields the highest CNR in the DWI ratio images.

We define the DWI ratio image as

$$\ln\left[\frac{S(b_1)}{S(b_2)}\right],$$

where $S(b_i)$ is the DWI signal intensity at $b=b_i$ and $b_1<b_2$.

We also use an IVIM model for modeling signal intensity on DWI such that $S(b) = S_0\,[(1-f)\cdot e^{-b\cdot D} + f\cdot e^{-b\cdot Dp}]$, where $S(b)$ is the signal intensity at b value, b, and S_0 is the fitted signal intensity at b=0. D is the pure tissue diffusion, D_p is the pseudo-diffusion coefficient due to blood flow and f is the perfusion fraction.

The expected CNR can be calculated as (see supplementary)

$$CNR = \frac{\mu_{\log\cdot r\cdot PZ}(b_1,b_2) - \mu_{\log\cdot r\cdot T}(b_1,b_2)}{\sqrt{\mathrm{var}_{\log\cdot r\cdot PZ}(b_1,b_2)}}, \quad [1]$$

where $\mu_{lg0\cdot r\cdot PZ}(b_1, b_2)$ and $\mu_{lg0\cdot r\cdot T}(b_1, b_2)$ are the mean signal on the DWI ratio image for peripheral zone and cancerous tissue, and $var_{lg0\cdot r\cdot PZ}(b_1, b_2)$ is the variance of the signal for the peripheral zone.

To determine the optimal high-low b value combinations, we selected low b values from b=0 to 500 with increments of 20 and high b values from b=500 to 2,000 with increments of 50. The CNR's were then calculated based on all possible high-low b value combinations. We also evaluated the CNR using a b value protocol mimicking that of the clinical mpMRI protocol at the authors' institution, where multiple acquisitions are averaged at high b values (see below).

The reference value for D, D_p, and f for prostate tissues were taken from (32) and listed in *Table 1* which were typical values as in the literature (33,34). The SNR at b=0 s/mm^2 was set at 10 and 20 to evaluate the impact of low or high image quality.

The institutional review board approved this retrospective analysis of patient data. This study was Health Insurance Portability and Accountability Act-compliant and the requirement of informed consent was waived. Men who underwent mpMRI of the prostate followed by radical prostatectomy for PCa between February/2014 and October/2014 were enrolled. Patients who met the following additional criteria were included in this study: index lesion seen on MRI, radical prostatectomy performed after MRI, and surgical pathology confirming a site-concordant index prostate acinar adenocarcinoma. Forty-three Consecutive men met eligibility criteria (*Figure 1*). Data from these patients were previously reported but the analysis and results of the data of the previous report do not overlap with this analysis (32). Patients with contraindication for MRI or unable to complete the MRI examination or who did not fulfill the inclusion criteria above were excluded from this study. Using the histopathologic profiles of radical prostatectomy specimens as the standard of reference, patients were stratified into low risk (Gleason score 6, or 3 + 4 with cancer in <20% of the prostate) (35), intermediate risk (Gleason score 3+4 with cancer in ≥20% of the prostate), and high risk (Gleason score ≥4+3) cancers (36). Such a risk can be interpreted as risk of being clinically significant cancer.

All patients underwent 3 T dual-transmit MRI exam with a 6-channel cardiac coil (Philips Healthcare, Best,

The Netherlands) and an endorectal coil (MEDRAD eCoil, Bayer Medical Care Inc., Indianola, PA, USA). Axial DWI were performed using a single-shot spin-echo echo-planar imaging sequence with fat suppression: TE/TR =80/7000 ms, FOV =160×180 mm^2, matrix =128×138, slice thickness/gaP =3/0.3 mm, 36 slices, b value (× number of averages)=0 (×1), 10 (×1), 25 (×1), 50 (×1), 100 (×1), 250 (×1), 450 (×1), 1,000 (×2), 1,500 (×3), and 2,000 (×5) s/mm^2, and scan time =6.5 min. The diffusion gradient was applied in three orthogonal directions to generate the trace diffusion-weighted images. ADC maps were created in the MRI scanner using a mono-exponential fitting and the following b values: 0, 100, 1,000, 1,500, and 2,000.

MRI examinations were reviewed on a commercially available workstation, VersaVue Enterprise (iCAD, Nashua, NH, USA). Based on the histopathologic results, the index lesion (37) was defined as the cancer focus with highest Gleason score in each patient; if the highest Gleason score was assigned to more than one lesion in the same patient, the index lesion was the largest lesion or the one associated with extra-prostatic extension if present (38). The index lesion was identified in each patient by a radiologist (DC, with 13 years of clinical prostate MRI experience) who was aware of the size and location of the index lesion at histopathology. A free-hand region of interest (ROI) was manually drawn on the ADC map generated from the scanner to delineate the cancer. Circular ROIs in the noncancerous peripheral zone were also drawn on the ADC map after confirmation of absence of cancer on those locations at histopathology. These ROIs were copied to the diffusion weighted images at the same slice locations to obtain the mean and standard deviation values of the PCa and noncancerous tissues. DWI ratio images were calculated as the ratio of the signals from the low b value image over the high b value image using a MATLAB script.

Based on the simulation results, DWI ratio images were calculated at the optimal b value combinations of R1 = b100/b1,000; R2 = b100/b1,500; and R3 = b100/b2,000). The CNRs were compared between DWI ratio images and ADC maps using a non-inferiority test with tolerance margin of 2 CNR. Friedman's two-way non-parametric Analysis of variance (ANOVA) was used with Post-hoc multiple comparison with Dunnett adjustment.

All DWI ratio images and ADC maps were anonymized and output into a DICOM viewer (OsiriX) in a random order. Two radiologists (G Khatri, T Yokoo) blinded to the image type (DWI ratio or ADC) independently rated the images for: (I) the presence of artifacts (lower the better); (II) cancer conspicuity (higher the better); and (III) overall image quality (higher the better) using a 5-point Likert scale. Reviewers were instructed to review all randomized images independently and were asked to keep their interpretation of the grading system consistent. For artifact, the reviewers graded the artifacts such as geometric distortion, signal graininess, ghosting artifacts and blurring. For cancer conspicuity, the reviewers assessed how good the lesion contrast to the background benign prostate tissue. For overall image quality, the reviewers gave an overall opinion of the quality of the image. Agreement between the readers was assessed by weighted kappa statistics. Agreement was considered as poor when kappa <0.4, fair to good when kappa >0.4 and <0.75 and excellent when kappa >0.75 (39). ANOVA with Dunnett adjustment was used to compare the difference in mean Likert scales between DWI ratio images and the ADC map. If either of the ratio images was found to have a lower score than ADC on average, a non-inferiority (to ADC map) test with tolerance margin of 0.5 point was used.

DWI ratio signals can be normalized into synthetic ADC due to their linear relationship by dividing the ratio signals by the difference between the two b values. The agreement between the synthetic ADC's and ADC maps from the scanner was assessed by intraclass correlations (ICC). Values less than 0.5, between 0.5 and 0.75, between 0.75 and 0.9, and greater than 0.90 are indicative of poor, moderate, good, and excellent reliability, respectively (40). Wilcoxon rank sum tests were used to test the difference between low and intermediate/high risk lesions on average.

Effects with P value of 0.05 or less was considered as statistically significant, in the context of noninferiority testing, the null hypotheses were the DWI ratio images were inferior to ADC maps by a predefined tolerance margin (δ). A P value of 0.05 or less can be interpreted as sufficient evidence that the DWI ratio images were no more than δ unites less than the ADC maps. SAS 9.4 (SAS Institute Inc., Cary, NC, USA) was used for statistical analysis.

Results

The reference values for pure tissue diffusion (*D*), pseudo-diffusion (*Dp*) and perfusion fraction (*f*) are listed in *Table 1*. Changes in CNR for different b value combinations are shown as heatmaps in *Figure 2*. Each point on the heatmap showed the expected CNR between normal tissue and lesion on a DWI ratio image based on the high-low b value

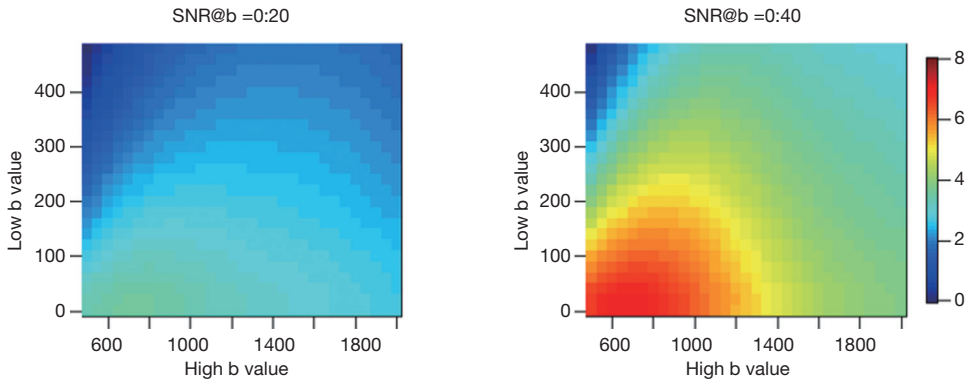

Figure 2 Heatmap of CNR for different high-low b value combinations on the DWI ratio image. Each point on the heatmap showed the expected CNR between normal tissue and lesion on a DWI ratio image based on the high-low b value combinations corresponding to its (x,y) coordinate. Higher CNR is shown as red and lower CNR was shown as blue. This is repeated in two noise settings: (I) SNR =20 at b= 0 s/mm^2; and (II) SNR =40 at b=0 s/mm^2. CNR, contrast-to-noise ratio; DWI, diffusion-weighted imaging; SNR, signal-to-noise ratio.

Table 2 Expected CNR using b value scheme in the clinical multiparametric MRI protocol

CNR, $SNR_{@b0}$ =20–40	Low b value						
	0 (×1)	10 (×1)	25 (×1)	50 (×1)	100 (×1)	250 (×1)	450 (×1)
High b value							
1,000 (×2)	4.5–8.6	4.5–8.6	4.4–8.6	4.4–8.4	4.1–8	3.3–6.4	2.2–4.4
1,500 (×3)	4.5–7.2	4.5–7.2	4.5–7.2	4.4–7.1	4.2–6.9	3.6–6	2.7–4.9
2,000 (×5)	5.3–7.5	5.3–7.5	5.2–7.5	5.2–7.4	4.9–7.2	4.1–6.4	3.1–5.4

CNR, contrast-to-noise ratio; MRI, magnetic resonance imaging; SNR, signal-to-noise ratio.

combinations corresponding to its (x,y) coordinate. This was repeated in two noise settings: (I) SNR =20 at b=0 s/mm^2 and (II) SNR =40 at b=0 s/mm^2. DWI ratio images constructed from a low b value ≤100 s/mm^2 against a high b value around 800 to 1,500 s/mm^2 had the highest CNR in our calculation for both noise settings.

Simulated CNR using a b value combination similar to that of the clinical mpMRI protocol at the authors' institution (i.e., with averaging of multiple acquisitions at high b values) are shown in *Table 2*. The CNR did not change appreciably when the low b value was <100 s/mm^2. On the other hand, a high b value of 2,000 s/mm^2 yielded a higher CNR than with a high b value of 1,000 s/mm^2.

A visual comparison between the conventional ADC map and the DWI ratio images is shown in *Figure 3*. Analysis of the quantitative data showed that DWI ratio images were not inferior to ADC maps by two units in CNR on average [P=0.0298 (ADC *vs.* R1), <0.0001 (ADC *vs.* R2) and <0.0001 (ADC *vs.* R3), *Table 3*].

On qualitative analysis, DWI ratio images had significantly lower artifacts than ADC maps on average [P=0.0007 (ADC *vs.* R1), 0.0003 (ADC *vs.* R2) and 0.0003 (ADC *vs.* R3), *Figure 4*]. Cancer conspicuity of R2 and R3 were no more than 0.5 point on Likert scale lower than that of the ADC maps on average [P=0.0895 (ADC *vs.* R1), 0.0128 (ADC *vs.* R2) and 0.0015 (ADC *vs.* R3)]. All ratio images were no more than 0.5 point on Likert scale lower than ADC in overall quality on average [P=0.0043 (ADC *vs.* R1), <0.0001 (ADC *vs.* R2), <0.0001 (ADC *vs.* R3), *Table 4*]. Reader agreement for the qualitative analysis was good to excellent [weighted kappa and 95% CI: Artifacts: 0.39 (0.25–0.53); cancer conspicuity: 0.72 (0.65–0.79); overall image quality: 0.64 (0.53–0.75)].

Agreement between ADC maps and the synthetic ADC's were excellent (*Figure 5*). Significant difference between low and intermediate/high risk were found in all measurements on average [P=0.005 (ADC), 0.013 (R1), 0.016 (R2) 0.033 (R3), *Table 5*, *Figure 6*].

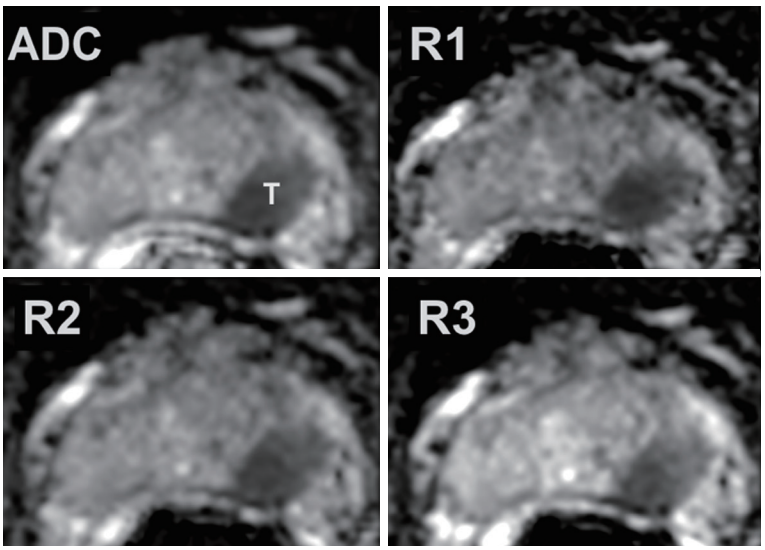

Figure 3 A 64-year-old man on active surveillance for Gleason 3+3 PCa. MRI reveals a highly suspicious lesion in the left mid peripheral zone, which is confirmed at surgery to be a Gleason 3+4 prostate cancer. Note the overall similar appearance of the images and, subjectively, the comparable tumor (T) conspicuity. MRI, magnetic resonance imaging; ADC, apparent diffusion coefficient from the mono-exponential model fit from the scanner; R1, DWI ratio image of b100/b1,000; R2, DWI ratio image of b100/b1,500; R3, DWI ratio image of b100/b2,000; DWI, diffusion-weighted imaging.

Table 3 A comparison of CNR between DWI ratio images and ADC maps

Variable	CNR	P values
ADC	5.72 (4.10–8.57)	–
R1	4.10 (2.98–6.59)	0.0298
R2	5.16 (3.64–6.87)	<0.0001
R3	5.11 (3.50–7.77)	<0.0001

Median (Q1–Q3), P values are for the non-inferiority test with tolerance margin of 2 units in CNR. CNR, contrast-to-noise ratio; DWI, diffusion-weighted imaging; ADC, apparent diffusion coefficient; R1, DWI ratio image of b100/b1,000; R2, DWI ratio image of b100/b1,500; R3, DWI ratio image of b100/b2,000.

Discussion

Bias in ADC estimation has been one of the major issues in the reproducibility of ADC. It is usually the result of (I) pseudo-diffusion effect at the low b values (<100 s/mm^2); (II) non-Gaussian signal distribution at high b values. More sophisticated models have been proposed to solve these two issues and provide more accurate estimates of the true tissue diffusion. But the calculation-complexity and the lack of robustness are all potential obstacles in preventing their integration into real-time clinical application (16). Further, a bias in ADC estimation by itself does not decrease the differentiability between normal and cancerous tissues within a patient (41,42). Algorithms such as the proposed DWI ratio image require far fewer b values, makes no assumption to the structure of the signal decay, and does not require iterative calculation for estimation. The model-independent nature of this approach also has the potential to improve inter-subject and inter-vendor reproducibility of DWI data for the detection and characterization of PCa when compared to ADC maps. A low b value at 100 s/mm^2 was also selected instead of b=0 s/mm^2 to avoid the influence of the pseudo-diffusion thus to increase the reproducibility.

The calculation of the DWI ratio image resembles the formula of ADC from a mono-exponential model with 2 b

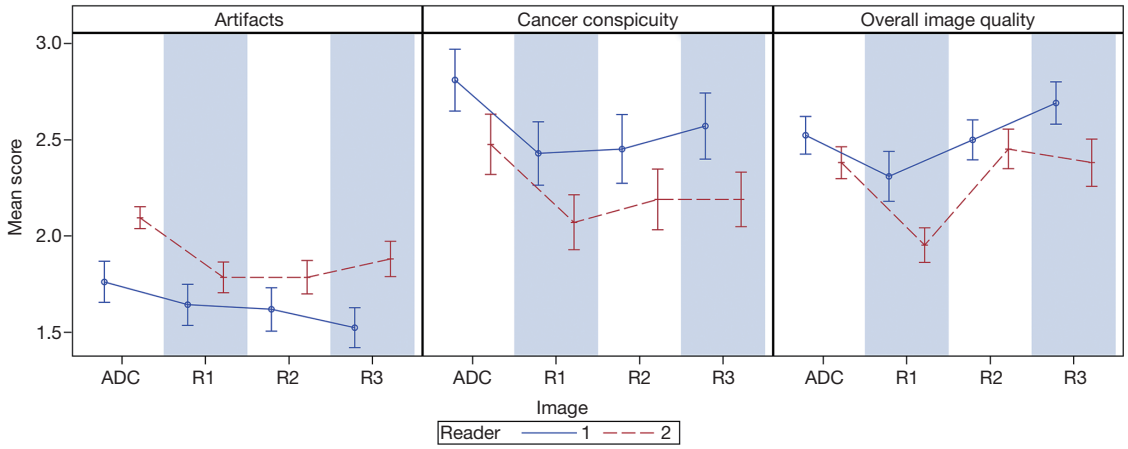

Figure 4 Qualitative assessment by two independent and blinded readers. ADC, apparent diffusion coefficient from the mono-exponential model fit from the scanner; R1, DWI ratio image of b100/b1,000; R2, DWI ratio image of b100/b1,500; R3, DWI ratio image of b100/b2,000; DWI, diffusion-weighted imaging.

Table 4 Qualitative 5-point Likert scores for different image datasets

Reader	Scores (mean ± SD)			
	ADC	R1	R2	R3
1				
Artifacts	1.76±0.69	1.64±0.69	1.62±0.73	1.52±0.67
Cancer conspicuity	2.81±1.04	2.43±1.06	2.45±1.15	2.57±1.11
Overall image quality	2.52±0.63	2.31±0.84	2.5±0.67	2.69±0.72
2				
Artifacts	2.12±0.45	1.79±0.52	1.79±0.56	1.88±0.59
Cancer conspicuity	2.48±1.02	2.07±0.92	2.19±1.02	2.19±0.92
Overall image quality	2.38±0.54	1.95±0.58	2.45±0.67	2.38±0.79

ADC, apparent diffusion coefficient; R1, DWI ratio image of b100/b1,000; R2, DWI ratio image of b100/b1,500; R3, DWI ratio image of b100/b2,000; DWI, diffusion-weighted imaging.

values also known as the 'Synthetic ADC' from (16)

$$ADC = \frac{\ln\left[\frac{S(Lb)}{S(Hb)}\right]}{Hb - Lb},$$

with *Lb* and *Hb* as the low and high 'key' b values and *S* as the signal intensity. Since the low and high b value is set a priori, the term *Hb–Lb* is redundant in the DWI ratio image calculation and was omitted as a result. The advantage of needing only 2 b values is that one can either (I) decrease the acquisition time by acquiring fewer images and maintain similar lesion conspicuity; or (II) increase the robustness of the DWI ratio image by acquiring more number of averages at high b values but keep the same scan time (as for conventional ADC maps).

Our results showed that a simple ratio of two DWI images with proper selection of the high-low b value combination was comparable to ADC map. The differentiability between normal and cancerous tissues was non-inferior to that of ADC map both quantitatively (CNR) and qualitatively (reader scores). In this study, b100/b1,500 and b100/b2,000 were the b value combinations yielding better results. The model-independent nature of this approach has the potential to improve inter-subject and

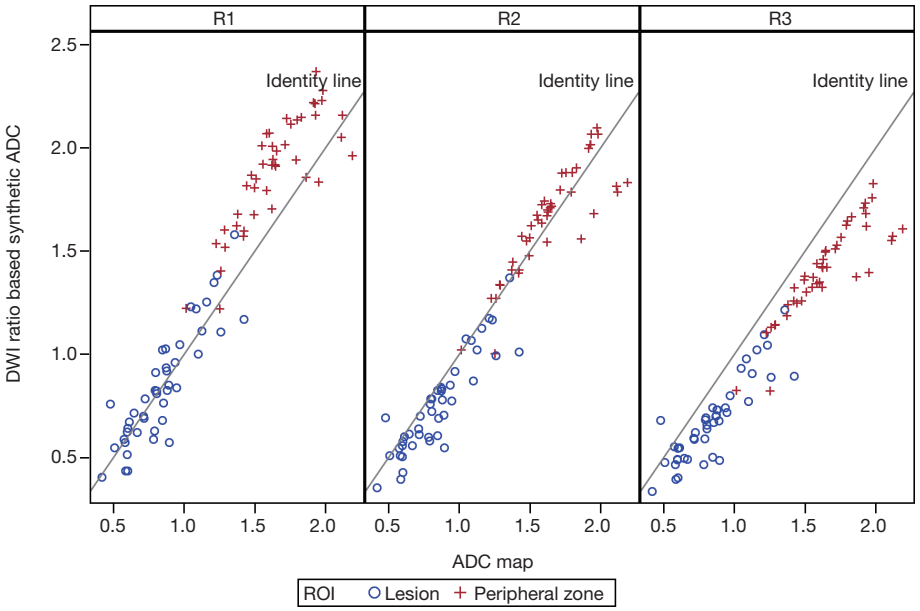

Figure 5 Scatter plots showing the agreement between the ADC map and DWI ratio based synthetic ADC. Cancers are marked as blue circles and uninvolved prostate tissues from the peripheral zone are marked as red cross. The identity line colored grey represents perfect match. Intraclass correlations were 0.94 (0.91–0.96) for ADC *vs.* R1, 0.946 (0.95–0.97) for ADC *vs.* R2 and 0.96 (0.94–0.97) for ADC *vs.* R3. ADC, apparent diffusion coefficient; DWI, diffusion-weighted imaging; R1, synthetic ADC based on b100/b1,000; R2, synthetic ADC based on b100/b1,500; R3, synthetic ADC based on b100/b2,000.

Table 5 Signal intensities for different lesion categories

Variable	Signal intensities, median (Q1–Q3)	
	Low risk	Intermediate/high risk
ADC	1.01 (0.87–1.2)	0.79 (0.6–0.88)
R1	1.11 (0.81–1.24)	0.77 (0.62–0.91)
R2	0.96 (0.71–1.1)	0.7 (0.56–0.78)
R3	0.85 (0.6–1)	0.63 (0.49–0.73)

ADC, apparent diffusion coefficient; R1, DWI ratio image of b100/b1,000; R2, DWI ratio image of b100/b1,500; R3, DWI ratio image of b100/b2,000; DWI, diffusion-weighted imaging.

inter-vendor reproducibility of DWI data for the detection and characterization of PCa when compared to ADC maps.

Our study has several limitations. First, it did not include a control group. It would be ideal to conduct a multi-reader double-blinded experiment with randomized normal and cancerous prostates to compare the diagnostic performance between state-of-the-art diffusion images (i.e., IVIM-kurtosis model) and our proposed DWI ratio image. Another limitation of the study was the lack of assessment of number of signal averages. The selection of the high b value is also sensitive to number of averages available. Third, the optimal b value selection for the DWI ratio image may be organ-specific. For cancer detection outside the prostate, a different set of optimal high-low b value combination needs to be determined. This can be seen as both an advantage and a disadvantage. On one hand, it is optimized for the target organ; but on the other hand, cancer detection in the nearby organs (metastasis) maybe compromised. Lastly, the present study was conducted using an endorectal coil protocol on a 3T system with a set number of acquisition averages. Generalizability of our results to non-endorectal coil and/or 1.5 T systems is unknown and further protocol-

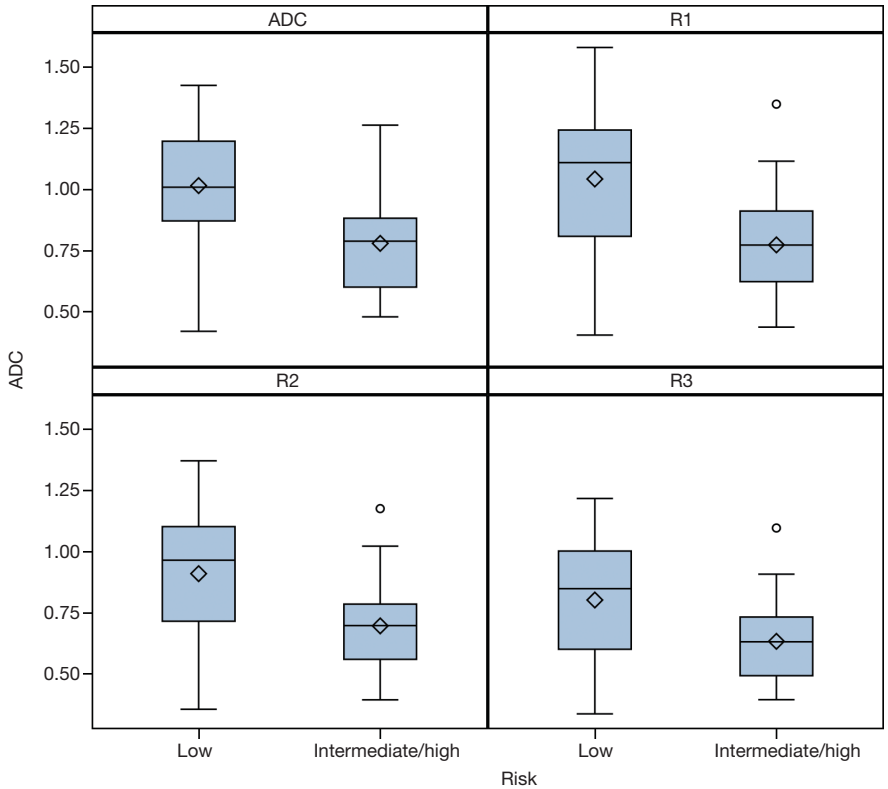

Figure 6 Boxplots of ADC and DWI ratio based synthetic ADC for low risk and intermediate/high risk cancers. ADC, apparent diffusion coefficient; DWI, diffusion-weighted imaging; R1, synthetic ADC based on b100/b1,000; R2, synthetic ADC based on b100/b1,500; R3, synthetic ADC based on b100/b2,000.

or platform-specific optimization may be needed.

In conclusion, we presented an analytical method for searching for the optimal combination of high and low b values for DWI ratio images in terms of minimizing CNR between cancer and surrounding benign tissues. The optimized DWI ratio images are model-independent alternative to ADC maps for the interpretation of DWI data in the context of prostate mpMRI.

Acknowledgements

None.

Footnote

Conflicts of Interest: The authors have no conflicts of interest to declare.

Ethical Statement: The study was approved by the institutional review board.

References

1. Padhani AR, Liu G, Koh DM, Chenevert TL, Thoeny HC, Takahara T, Dzik-Jurasz A, Ross BD, Van Cauteren M, Collins D, Hammoud DA, Rustin GJ, Taouli B, Choyke PL. Diffusion-weighted magnetic resonance imaging as a cancer biomarker: consensus and recommendations. Neoplasia 2009;11:102-25.
2. Taouli B, Beer AJ, Chenevert T, Collins D, Lehman C, Matos C, Padhani AR, Rosenkrantz AB, Shukla-Dave A, Sigmund E, Tanenbaum L, Thoeny H, Thomassin-Naggara I, Barbieri S, Corcuera-Solano I, Orton M, Partridge SC, Koh DM. Diffusion-weighted imaging outside the brain: Consensus statement from an ISMRM-sponsored workshop. J Magn Reson Imaging 2016;44:521-40.
3. Pang Y, Turkbey B, Bernardo M, Kruecker J, Kadoury S, Merino MJ, Wood BJ, Pinto PA, Choyke PL. Intravoxel incoherent motion MR imaging for prostate cancer: An evaluation of perfusion fraction and diffusion coefficient derived from different b value combinations. Magn Reson

Med 2013;69:553-62.
4. Haider MA, Yao X, Loblaw A, Finelli A. Multiparametric Magnetic Resonance Imaging in the Diagnosis of Prostate Cancer: A Systematic Review. Clin Oncol (R Coll Radiol) 2016;28:550-67.
5. Fusco R, Sansone M, Granata V, Setola SV, Petrillo A. A systematic review on multiparametric MR imaging in prostate cancer detection. Infect Agent Cancer 2017;12:57.
6. Futterer JJ. Multiparametric MRI in the Detection of Clinically Significant Prostate Cancer. Korean J Radiol 2017;18:597-606.
7. Shaish H, Kang SK, Rosenkrantz AB. The utility of quantitative ADC values for differentiating high-risk from low-risk prostate cancer: a systematic review and meta-analysis. Abdom Radiol (NY) 2017;42:260-70.
8. Turkbey B, Shah VP, Pang YX, Bernardo M, Xu S, Kruecker J, Locklin J, Baccala AA, Rastinehad AR, Merino MJ, Shih JH, Wood BJ, Pinto PA, Choyke PL. Is Apparent Diffusion Coefficient Associated with Clinical Risk Scores for Prostate Cancers that Are Visible on 3-T MR Images? Radiology 2011;258:488-95.
9. Tamada T, Sone T, Jo Y, Yamamoto A, Yamashita T, Egashira N, Imai S, Fukunaga M. Prostate cancer: Relationships between postbiopsy hemorrhage and tumor detectability at MR diagnosis. Radiology 2008;248:531-9.
10. Woodfield CA, Tung GA, Grand DJ, Pezzullo JA, Machan JT, Renzulli JF. Diffusion-Weighted MRI of Peripheral Zone Prostate Cancer: Comparison of Tumor Apparent Diffusion Coefficient With Gleason Score and Percentage of Tumor on Core Biopsy. AJR Am J Roentgenol 2010;194:W316-22.
11. Lebihan D, Breton E, Lallemand D, Aubin ML, Vignaud J, Lavaljeantet M. Separation of Diffusion and Perfusion in Intravoxel Incoherent Motion Mr Imaging. Radiology 1988;168:497-505.
12. Kuru TH, Roethke MC, Stieltjes B, Maier-Hein K, Schlemmer HP, Hadaschik BA, Fenchel M. Intravoxel Incoherent Motion (IVIM) Diffusion Imaging in Prostate Cancer - What Does It Add? J Comput Assist Tomogr 2014;38:558-64.
13. Shinmoto H, Oshio K, Tamura C, Soga S, Okamura T, Yamada K, Kaji T, Mulkern RV. Diffusion-weighted imaging of prostate cancer using a statistical model based on the gamma distribution. J Magn Reson Imaging 2015;42:56-62.
14. Rosenkrantz AB, Sigmund EE, Johnson G, Babb JS, Mussi TC, Melamed J, Taneja SS, Lee VS, Jensen JH. Prostate cancer: feasibility and preliminary experience of a diffusional kurtosis model for detection and assessment of aggressiveness of peripheral zone cancer. Radiology 2012;264:126-35.
15. Jensen JH, Helpern JA. MRI quantification of non-Gaussian water diffusion by kurtosis analysis. NMR Biomed 2010;23:698-710.
16. Iima M, Le Bihan D. Clinical Intravoxel Incoherent Motion and Diffusion MR Imaging: Past, Present, and Future. Radiology 2016;278:13-32.
17. Kitajima K, Takahashi S, Ueno Y, Yoshikawa T, Ohno Y, Obara M, Miyake H, Fujisawa M, Sugimura K. Clinical utility of apparent diffusion coefficient values obtained using high b value when diagnosing prostate cancer using 3 tesla MRI: comparison between ultra-high b value (2000 s/mm(2)) and standard high b value (1000 s/mm(2)). J Magn Reson Imaging 2012;36:198-205.
18. Manenti G, Nezzo M, Chegai F, Vasili E, Bonanno E, Simonetti G. DWI of Prostate Cancer: Optimal b value in Clinical Practice. Prostate Cancer 2014;2014:868269.
19. Rosenkrantz AB, Hindman N, Lim RP, Das K, Babb JS, Mussi TC, Taneja SS. Diffusion-weighted imaging of the prostate: Comparison of b1000 and b2000 image sets for index lesion detection. J Magn Reson Imaging 2013;38:694-700.
20. Ueno Y, Kitajima K, Sugimura K, Kawakami F, Miyake H, Obara M, Takahashi S. Ultra-high b value diffusion-weighted MRI for the detection of prostate cancer with 3-T MRI. J Magn Reson Imaging 2013;38:154-60.
21. Kim CK, Park BK, Kim B. High-b value diffusion-weighted imaging at 3 T to detect prostate cancer: comparisons between b values of 1,000 and 2,000 s/mm^2. AJR Am J Roentgenol 2010;194:W33-7.
22. Ogura A, Koyama D, Hayashi N, Hatano I, Osakabe K, Yamaguchi N. Optimal b Values for Generation of Computed High-b value DW Images. AJR Am J Roentgenol 2016;206:713-8.
23. Ohgiya Y, Suyama J, Seino N, Hashizume T, Kawahara M, Sai S, Saiki M, Munechika J, Hirose M, Gokan T. Diagnostic accuracy of ultra-high-b value 3.0-T diffusion-weighted MR imaging for detection of prostate cancer. Clin Imaging 2012;36:526-31.
24. Tamada T, Kanomata N, Sone T, Jo Y, Miyaji Y, Higashi H, Yamamoto A, Ito K. High b value (2,000 s/mm^2) diffusion-weighted magnetic resonance imaging in prostate cancer at 3 Tesla: comparison with 1,000 s/mm^2 for tumor conspicuity and discrimination of aggressiveness. PLoS One 2014;9:e96619.
25. Metens T, Miranda D, Absil J, Matos C. What is the

optimal b value in diffusion-weighted MR imaging to depict prostate cancer at 3T? Eur Radiol 2012;22:703-9.
26. Maas MC, Futterer JJ, Scheenen TW. Quantitative evaluation of computed high B value diffusion-weighted magnetic resonance imaging of the prostate. Invest Radiol 2013;48:779-86.
27. Agarwal HK, Mertan FV, Sankineni S, Bernardo M, Senegas J, Keupp J, Daar D, Merino M, Wood BJ, Pinto PA, Choyke PL, Turkbey B. Optimal high b value for diffusion weighted MRI in diagnosing high risk prostate cancers in the peripheral zone. J Magn Reson Imaging 2017;45:125-31.
28. Rosenkrantz AB, Mannelli L, Kong X, Niver BE, Berkman DS, Babb JS, Melamed J, Taneja SS. Prostate cancer: utility of fusion of T2-weighted and high b value diffusion-weighted images for peripheral zone tumor detection and localization. J Magn Reson Imaging 2011;34:95-100.
29. Le Bihan D, Breton E, Lallemand D, Aubin ML, Vignaud J, Laval-Jeantet M. Separation of diffusion and perfusion in intravoxel incoherent motion MR imaging. Radiology 1988;168:497-505.
30. Le Bihan D, Breton E, Lallemand D, Grenier P, Cabanis E, Laval-Jeantet M. MR imaging of intravoxel incoherent motions: application to diffusion and perfusion in neurologic disorders. Radiology 1986;161:401-7.
31. Grant KB, Agarwal HK, Shih JH, Bernardo M, Pang Y, Daar D, Merino MJ, Wood BJ, Pinto PA, Choyke PL, Turkbey B. Comparison of calculated and acquired high b value diffusion-weighted imaging in prostate cancer. Abdom Imaging 2015;40:578-86.
32. Yuan Q, Costa DN, Senegas J, Xi Y, Wiethoff AJ, Rofsky NM, Roehrborn C, Lenkinski RE, Pedrosa I. Quantitative diffusion-weighted imaging and dynamic contrast-enhanced characterization of the index lesion with multiparametric MRI in prostate cancer patients. J Magn Reson Imaging 2017;45:908-16.
33. Tamada T, Prabhu V, Li J, Babb JS, Taneja SS, Rosenkrantz AB. Prostate Cancer: Diffusion-weighted MR Imaging for Detection and Assessment of Aggressiveness-Comparison between Conventional and Kurtosis Models. Radiology 2017;284:100-8.
34. Yoshizako T, Wada A, Hayashi T, Uchida K, Sumura M, Uchida N, Kitagaki H, Igawa M. Usefulness of diffusion-weighted imaging and dynamic contrast-enhanced magnetic resonance imaging in the diagnosis of prostate transition-zone cancer. Acta Radiol 2008;49:1207-13.
35. Ramos CG, Roehl KA, Antenor JA, Humphrey PA, Catalona WJ. Percent carcinoma in prostatectomy specimen is associated with risk of recurrence after radical prostatectomy in patients with pathologically organ confined prostate cancer. J Urol 2004;172:137-40.
36. Stark JR, Perner S, Stampfer MJ, Sinnott JA, Finn S, Eisenstein AS, Ma J, Fiorentino M, Kurth T, Loda M, Giovannucci EL, Rubin MA, Mucci LA. Gleason score and lethal prostate cancer: does 3 + 4 = 4 + 3? J Clin Oncol 2009;27:3459-64.
37. Ahmed HU. The index lesion and the origin of prostate cancer. N Engl J Med 2009;361:1704-6.
38. Weinreb JC, Barentsz JO, Choyke PL, Cornud F, Haider MA, Macura KJ, Margolis D, Schnall MD, Shtern F, Tempany CM, Thoeny HC, Verma S. PI-RADS Prostate Imaging - Reporting and Data System: 2015, Version 2. Eur Urol 2016;69:16-40.
39. Senn S. Review of Fleiss, statistical methods for rates and proportions. Res Synth Methods 2011;2:221-2.
40. Koo TK, Li MY. A Guideline of Selecting and Reporting Intraclass Correlation Coefficients for Reliability Research. J Chiropr Med 2016;15:155-63.
41. Moldovan PC, Van den Broeck T, Sylvester R, Marconi L, Bellmunt J, van den Bergh RCN, Bolla M, Briers E, Cumberbatch MG, Fossati N, Gross T, Henry AM, Joniau S, van der Kwast TH, Matveev VB, van der Poel HG, De Santis M, Schoots IG, Wiegel T, Yuan CY, Cornford P, Mottet N, Lam TB, Rouviere O. What Is the Negative Predictive Value of Multiparametric Magnetic Resonance Imaging in Excluding Prostate Cancer at Biopsy? A Systematic Review and Meta-analysis from the European Association of Urology Prostate Cancer Guidelines Panel. Eur Urol 2017;72:250-66.
42. Quentin M, Blondin D, Klasen J, Lanzman RS, Miese FR, Arsov C, Albers P, Antoch G, Wittsack HJ. Comparison of different mathematical models of diffusion-weighted prostate MR imaging. Magn Reson Imaging 2012;30:1468-74.

Cite this article as: Xi Y, Liu A, Olumba F, Lawson P, Costa DN, Yuan Q, Khatri G, Yokoo T, Pedrosa I, Lenkinski RE. Low-to-high b value DWI ratio approaches in multiparametric MRI of the prostate: feasibility, optimal combination of b values, and comparison with ADC maps for the visual presentation of prostate cancer. Quant Imaging Med Surg 2018;8(6):557-567. doi: 10.21037/qims.2018.06.08

Supplementary

Derivation of the contrast-to-noise ratio between peripheral zone and cancerous tissue on the DWI ratio image.

Given D, f, D_p and S_0 from the literature for peripheral zone and cancer, the signal intensity at b value, b, can be calculated as,

$$\begin{cases} S_{PZ}(b) = S_{0\,pz}\left[\left(1-f_{pz}\right)\cdot e^{-b\cdot D_{pz}} + f\cdot e^{-b\cdot D_{p\,pz}}\right] \\ S_T(b) = S_{0T}\left[\left(1-f_T\right)\cdot e^{-b\cdot D_T} + f\cdot e^{-b\cdot D_{p\,T}}\right] \end{cases},$$

where PZ stands for peripheral zone and T stands for cancer. With Rician noise (43,44) and scale parameter σ (which can be determined by the signal-to-noise ratio (SNR) at b=0), the expected values (μ) and variances (var) for PZ and cancer are

$$\mu_{PZ}(b) = \sigma\sqrt{\frac{\pi}{2}}L_{\frac{1}{2}}\left(-\frac{S_{PZ}^2(b)}{2\sigma^2}\right),$$

$$\mathrm{var}_{PZ}(b) = 2\sigma^2 + S_{PZ}^2(b) - \frac{\pi\sigma^2}{2}L_{\frac{1}{2}}^2\left(-\frac{S_{PZ}^2(b)}{2\sigma^2}\right),$$

$$\mu_T(b) = \sigma\sqrt{\frac{\pi}{2}}L_{\frac{1}{2}}\left(-\frac{S_T^2(b)}{2\sigma^2}\right),$$

$$\mathrm{var}_T(b) = 2\sigma^2 + S_T^2(b) - \frac{\pi\sigma^2}{2}L_{\frac{1}{2}}^2\left(-\frac{S_T^2(b)}{2\sigma^2}\right).$$

Next, we calculate the mean and variance for PZ and cancer on the DWI ratio images. Let b_1 and b_2 be two b values such that $b_1<b_2$. Then the expected values on the ratio image can be approximated with first-order Taylor expansion as (45)

$$\mu_{r\cdot PZ}(b_1,b_2) \approx \frac{\mu_{PZ}(b_1)}{\mu_{PZ}(b_2)},$$

$$\mu_{r\cdot T}(b_1,b_2) \approx \frac{\mu_T(b_1)}{\mu_T(b_2)}.$$

with corresponding variance of the ratios for PZ (assuming independence)

$$\mathrm{var}_{r\cdot PZ}(b_1,b_2) \approx \frac{\mu_{PZ}^2(b_1)}{\mu_{PZ}^2(b_2)}\left[\frac{\mathrm{var}_{PZ}(b_1)}{\mu_{PZ}^2(b_1)} + \frac{\mathrm{var}_{PZ}(b_2)}{\mu_{PZ}^2(b_2)}\right].$$

Using Taylor expansion, again, mean and variance on the log of the ratios are approximated as

$$\mu_{\log\cdot r\cdot PZ}(b_1,b_2) \approx \log\left[\mu_{r\cdot PZ}(b_1,b_2)\right] + \frac{1}{\mu_{r\cdot PZ}(b_1,b_2)^2}\mathrm{var}_{r\cdot PZ}(b_1,b_2),$$

$$\mu_{\log\cdot r\cdot T}(b_1,b_2) \approx \log\left[\mu_{r\cdot T}(b_1,b_2)\right] + \frac{1}{\mu_{r\cdot T}(b_1,b_2)^2}\mathrm{var}_{r\cdot T}(b_1,b_2),$$

$$\mathrm{var}_{\log\cdot r\cdot PZ}(b_1,b_2) \approx \frac{1}{\mu_{r\cdot PZ}(b_1,b_2)^2}\mathrm{var}_{r\cdot PZ}(b_1,b_2).$$

Finally, we calculate the analytical approximation of contrast-to-noise ratio as

$$CNR = \frac{\mu_{\log\cdot r\cdot PZ}(b_1,b_2) - \mu_{\log\cdot r\cdot T}(b_1,b_2)}{\sqrt{\mathrm{var}_{\log\cdot r\cdot PZ}(b_1,b_2)}}.$$

References

43. Andersen AH. On the Rician distribution of noisy MRI data. Magn Reson Med 1996;36:331-3.
44. Gudbjartsson H, Patz S. The Rician distribution of noisy MRI data. Magn Reson Med 1995;34:910-4.
45. Casella G, Berger RL. Statistical inference. 2nd ed. Australia; Pacific Grove, CA: Thomson Learning, 2002:xxviii, 660.